Wrinkling analysis of pre-stressed membranes using element free Galerkin method

K R Unnikrishnan[1], C O Arun[2], and I R Praveen Krishna[3]

[1]Tata Consultancy Services Pune
[2]Indian Institute of Space Science and Technology

ABSTRACT

In the current study, element free Galerkin method, a meshless method, is proposed for wrinkling analysis of pre-stressed membranes. The mathematical model for studying wrinkling of pre-stressed membranes is derived by considering the bending stiffness, though it is negligible. Moving least approximation for deflection is constructed by considering three degrees of freedom per node. Essential boundary conditions are imposed using scaled transformation matrix method. Initially, compression induced wrinkling of a homogeneous thin plate without pre-stress is solved to validate the method and then a pre-stressed homogeneous membrane is analyzed for both compression induced and shear induced wrinkling. Capabilities of proposed method for membrane analysis is compared with that of finite element method(FEM). Comparative study on wrinkling analysis using EFGM and different FEM element types in a FEM package shows that, in lower modes both methods shows satisfying consistency in eigenvalues with respect to total of number of nodes, while at higher modes EFGM shows better consistency than FEM. Further the study is extended to wrinkling of non-homogeneous membranes subjected to linearly varying in-plane load. The results obtained from EFGM analysis is compared and found to be matching well with those available in literature.

INTRODUCTION

Thin membranes are largely used in the field of aerospace engineering applications such as solar collectors, parachutes, sun-shield, antennae, balloons, space radars, solar sails [1, 2] etc, because of its light weight and low space requirements. In most of these applications, the membrane will be kept folded and deployed to the required shape at the time of application. This process may produce wrinkles in the membrane as it has very small bending rigidity. Also, due to its lower bending stiffness, it cannot support compressive and bending loads. Most of the application needs highly smooth surface without wrinkles, in order to have maximum efficiency. This is usually achieved by giving a pre-stressing in the plane of the sheet. However, though these are pre-stressed, chances of wrinkling due to various loads acting on the membranes still exists.

A large number of studies are available in the area of membrane analysis [3, 4, 5, 6, 7, 8, 9, 10, 11, 12, 13, 14]. Tension field theory [3] and bifurcation analysis [15] are two early developed approaches used in wrinkling analysis. Wagner[3] proposed the tension field theory for the wrinkling problem and estimated the maximum shear load that can be carried by a membrane. Wong and Pellegrino[10, 11, 12], conducted experimental and analytical studies on shear induced wrinkling of rectangular membrane and verified it numerically using FEM. Also they have extended their research into wrinkling due to corner loads on a square plate.

Miyamura[16] studied wrinkling of pre-stressed circular membrane due to in-plane torsional load. Stress in the membrane are found from experiments and are compared with the results obtained from bifurcation analysis. Xiao et al.[13] analyzed wrinkles on a square planar thin film under pure shear and validated using experimental results. The influence of shear force, pre-stress and boundary conditions were also investigated. Kumar et al.[14] studied wrinkling of a membrane due to tensile and shear loading using commercial finite element package ABAQUS. The work was concentrated on the variation in eigenvalues and number of wrinkles with thickness and aspect ratios for different materials. Leissa et al.[17] found exact solution for buckling and vibration of thin plate, having two opposite edges simply supported and other two edges clamped, subjected to linearly varying in-plane load, using power series method. They extended the studies to other boundary conditions as well [18]. Wang et al.[19] used differential quadrature (DQ) technique to solve the plate buckling problems studied by Leissa et al.[17]. Lal and Saini[20] studied buckling and vibration analysis of non-homogeneous thin plates subjected to linearly varying in-plane loads using DQ method. The variation of critical load with various parameters like a/b ratio, non homogeneity parameter, loading parameter etc were studied. Though there exist a number of analytical, empirical and numerical studies, currently the most common practice in structural analysis is the use of FEM with the help of any commercially available packages. FEM, due to its simplicity and robustness, found its way into both industrial and academic fields. Also there are works on wrinkling analysis of membranes using FEM [12, 21]. However, use of non-conforming shell/plate elements available in commercial FEM softwares can lead to erroneous eigenvalues [22, 23]. Very small thickness of membranes also play a role in restricting the use of regular FEM plate/shell elements [22] and make the analysis cumbersome. Moreover, wrinkling is a highly mesh dependent problem and hence usage of FEM invites high computational time and cost. One way of handling these complexities is to re-mesh the problem domain at every stage or to refine mesh on that particular area. This helps in preventing severe distortion of element and also deals with the discontinuities developed at each stage. However, these are computationally expensive and less accurate. The use of very fine elements also leads to generation of localized modes in problems like wrinkling, vibration etc. Meshless methods are another way of avoiding the difficulties associated with FEM such as high cost in meshing low accuracy in stress difficulty in adaptive analysis etc [24], by alleviating the discretization of problem domain into elements or meshes. Only a set of nodes scattered on the problem domain are needed to represent the problem domain. The main advantage of these methods is its simplicity in adaptive analysis and problems with moving boundary discontinuities.

Among these meshless methods, the EFGM is particularly simple and has faster rate of convergence [25, 26, 27]. EFGM uses moving least square (MLS) method [28] for approximating the function. Krysl and Belytschko[29] introduced EFGM to the bending analysis of thin plates using Kirchhoff thin plate theory and extended the same to the analysis of thin shells [30]. EFGM had been used for vibration analysis of beams, plates and shells [31, 32, 33]. Enforcing essential boundary conditions in EFGM is little complicated when compared to methods like FEM. This is owing to lack of Kronecker delta property of MLS shape functions. Several techniques like, Lagrange multiplier [25], penalty function [34], scaled transformation method [27] etc are used to address this issue. For the current paper scaled transformation method is used for enforcing essential boundary conditions. Overall EFGM is found to be computationally efficient tool in many engineering applications. However, wrinkling analysis of pre-stressed membranes and non-homogeneous membranes using EFGM or any other meshless methods is missing in the available literature.

The current study proposes to use EFGM for wrinkling analysis of pre-stressed membranes.

In the proposed approach, governing differential equation is derived by coupling bending stiffness along with membrane forces using the principles of Love- Kirchoff thin plate theory. Though the present work does not do a study on post wrinkling behavior or study on effect permanent folding lines which necessitate the incorporation of bending stiffness [22], thin plate bending theory is used to obtain more general and simple mathematical model. The proposed method uses a deflection approximation with three degree of freedom (DOF) per node for MLS. The capabilities of EFGM in wrinkling of membrane is examined through different examples. In the first case, wrinkling analysis of a homogeneous membrane, without pre-stress is solved using EFGM and results are compared with those obtained analytically and from FEM. Wrinkling due to compressive loading and due to shear loading of a pre-stressed membrane is studied in the second problem. The results obtained from both these problems are compared with FEM, using different element types available. The dependency of eigenvalues on the number of nodes are studied and a convergence study is also conducted with the different element types and EFGM. In the third case, wrinkling of a non-homogeneous membrane subjected to linearly varying uni-axial load is studied. The results obtained are compared with the solutions available in the literature.

VARIATIONAL FORMULATION FOR MEMBRANE WRINKLING

The governing differential equation of an initially flat, isotropic, non-homogeneous thin membrane defined on a $x-y$ Cartesian plane; assuming classical plate theory for incorporating the flexural rigidity and considering in-plane forces is given by,

$$\frac{\partial^2 M_x}{\partial x^2} - 2\frac{\partial^2 M_{xy}}{\partial x \partial y} + \frac{\partial^2 M_y}{\partial y^2} = F_x\left(\frac{\partial^2 w}{\partial x^2}\right) + F_y\left(\frac{\partial^2 w}{\partial y^2}\right) + 2F_{xy}\left(\frac{\partial^2 w}{\partial x \partial y}\right), \tag{1}$$

where M_x, M_y are bending moments with respect to y, x axis and M_{xy} is the twisting moment, given by,

$$\begin{aligned} M_x &= -D(x,y)\left[\frac{\partial^2 w}{\partial x^2} + \nu\frac{\partial^2 w}{\partial y^2}\right] \\ M_y &= -D(x,y)\left[\frac{\partial^2 w}{\partial y^2} + \nu\frac{\partial^2 w}{\partial x^2}\right] \\ M_{xy} &= D(x,y)(1-\nu)\frac{\partial^2 w}{\partial x \partial y}, \end{aligned} \tag{2}$$

where w is the deflection in z direction, F_x, F_y are in plane loads per unit length in x, y direction and F_{xy} is shear load per unit length acting on the middle plane of the membrane. $D(x,y)$ is membrane flexural rigidity defined as,

$$D(x,y) = \frac{E(x,y)h^3}{12(1-\nu^2)}, \tag{3}$$

where h is thickness of membrane and $E(x,y)$ is modulus of elasticity, and ν is Poisson's ratio, which is assumed to be constant. The increment in the total potential energy of the thin plate upon buckling is given by [35],

$$\begin{aligned} \Delta\Pi = \frac{1}{2}\iint_A D\Big[\Big(\frac{\partial^2 w}{\partial x^2} + \frac{\partial^2 w}{\partial y^2}\Big)^2 + 2(1-\nu)\Big[\Big(\frac{\partial^2 w}{\partial x \partial y}\Big)^2 - \frac{\partial^2 w}{\partial x^2}\frac{\partial^2 w}{\partial y^2}\Big)\Big]dxdy \\ + \frac{1}{2}\int_0^a \int_0^b \Big[F_x\Big(\frac{\partial w}{\partial x}\Big)^2 + F_y\Big(\frac{\partial w}{\partial y}\Big)^2 + 2F_{xy}\Big(\frac{\partial w}{\partial x}\frac{\partial w}{\partial y}\Big)\Big]dxdy. \end{aligned} \tag{4}$$

Equation 4 is solved using EFGM as explained in the following sections.

EFGM FORMULATION

In EFGM, the unknown field variable $\mathbf{w}^h(\mathbf{x})$ can be written as[25].,

$$\mathbf{w}^h(\mathbf{x}) = \sum_{i=1}^{m} p_i(x)a_i(x) = \mathbf{p}^T(\mathbf{x})\mathbf{a}(\mathbf{x}), \tag{5}$$

where $\mathbf{p}^T(\mathbf{x})$ is the basis function of order m and $\mathbf{a(x)}$ are the unknown coefficients which depends on the position $\mathbf{x}$. To model thin membrane using Love-Kirchhoff's plate assumption, a quadratic basis function is used, which is given by,$\mathbf{p}^T(\mathbf{x}) = \begin{Bmatrix} 1 & x & y & x^2 & xy & y^2 \end{Bmatrix}$

The unknown coefficients at any point $\mathbf{x}$, are determined by performing a weighted least square fit of the local approximation, which in turn determined by minimizing the difference between local approximation at that point and nodal parameters [26]. A support domain or domain of influence is considered such that the weight function chosen has finite value inside this domain and has a value zero outside. A rectangular domain of influence is considered here[26]. Weight function of cubic type [24] is used for the present study Here in case of thin membrane wrinkling, considering three DOF per node, $\mathcal{L}2$ norm can be defined as,

$$J = \sum_{i}^{n} W(\mathbf{x} - \mathbf{x}_i)\Big\{[\mathbf{p}^T(\mathbf{x}_i)\mathbf{a}(\mathbf{x}) - w_i]^2 + [\mathbf{p}_{,y}{}^T(\mathbf{x}_i)\mathbf{a}(\mathbf{x}) - \theta_{xi}]^2 + [\mathbf{p}_{,x}{}^T(\mathbf{x}_i)\mathbf{a}(\mathbf{x}) - \theta_{yi}]^2\Big\}, \tag{6}$$

where $W(\mathbf{x} - \mathbf{x}_i)$ is the weight function, n is the number of nodes inside domain of influence and θ_x,θ_y are rotation in x, y direction respectively. The unknown coefficients can be found out by minimizing the $\mathcal{L}2$ norm. By differentiating J with respect to a_j,

$$\begin{aligned} \frac{\partial J}{\partial a_j} = \sum_{i}^{n} W(x - x_i)\Big\{ & p_j(\mathbf{x}_i)[\mathbf{p}^T(\mathbf{x}_i)\mathbf{a}(\mathbf{x}) - w_i] + p_{j,y}(\mathbf{x_i})[\mathbf{p}_{,y}^T(\mathbf{x}_i)\mathbf{a}(\mathbf{x}) - \theta_{xi}] \\ & + p_{j,x}(\mathbf{x_i})[\mathbf{p}_{,x}{}^T(\mathbf{x}_i)\mathbf{a}(\mathbf{x}) - \theta_{yi}]\Big\} = 0, \\ & j = 1, 2, 3....m \end{aligned} \tag{7}$$

Assembling all j and representing in matrix form,

$$\mathbf{A(x)a(x)=C(x)}. \tag{8}$$

where, $\mathbf{A}(\mathbf{x})$ is called the weighted moment matrix [24] defined by,

$$\mathbf{A}(\mathbf{x}) = \sum_{i=1}^{n} W_i(x - x_i)[\mathbf{p}(\mathbf{x}_i)\mathbf{p}^T(\mathbf{x}_i) + \mathbf{p}_{,y}(\mathbf{x}_i)\mathbf{p}_{,y}{}^T(\mathbf{x}_i) + \mathbf{p}_{,x}(\mathbf{x}_i)\mathbf{p}_{,x}{}^T(\mathbf{x}_i)], \tag{9}$$

$\mathbf{C(x)}$ is given by,

$$\mathbf{C(x)} = \mathbf{C_w w} + \mathbf{C}_{\theta_\mathbf{x}}\theta_\mathbf{x} + \mathbf{C}_{\theta_\mathbf{y}}\theta_\mathbf{y}, \tag{10}$$

with,

$$
\begin{aligned}
\mathbf{C}_{\mathbf{w}} &= \begin{bmatrix} W(\mathbf{x}-\mathbf{x}_1)\mathbf{p}(\mathbf{x}_1) & W(\mathbf{x}-\mathbf{x}_2)\mathbf{p}(\mathbf{x}_2) & . & . & . & W(\mathbf{x}-\mathbf{x}_n)\mathbf{p}(\mathbf{x}_n) \end{bmatrix} \\
\mathbf{C}_{\theta_{\mathbf{x}}} &= \begin{bmatrix} W(\mathbf{x}-\mathbf{x}_1)\mathbf{p}_{,y}(\mathbf{x}_1) & W(\mathbf{x}-\mathbf{x}_2)\mathbf{p}_{,y}(\mathbf{x}_2) & . & . & . & W(\mathbf{x}-\mathbf{x}_n)\mathbf{p}_{,y}(\mathbf{x}_n) \end{bmatrix} \\
\mathbf{C}_{\theta_{\mathbf{y}}} &= \begin{bmatrix} W(\mathbf{x}-\mathbf{x}_1)\mathbf{p}_{,x}(\mathbf{x}_1) & W(\mathbf{x}-\mathbf{x}_2)\mathbf{p}_{,x}(\mathbf{x}_2) & . & . & . & W(\mathbf{x}-\mathbf{x}_n)\mathbf{p}_{,x}(\mathbf{x}_n) \end{bmatrix} \\
&.
\end{aligned} \tag{11}
$$

From equation 8 and equation 10, $\mathbf{a}(\mathbf{x})$ can be obtained as,

$$
\mathbf{a}(\mathbf{x}) = \mathbf{A}(\mathbf{x})^{-1}[\mathbf{C}_{\mathbf{w}}\mathbf{w} + \mathbf{C}_{\theta_{\mathbf{x}}}\theta_{\mathbf{x}} + \mathbf{C}_{\theta_{\mathbf{y}}}\theta_{\mathbf{y}}]. \tag{12}
$$

Finally, substituting equation 12 in equation 5, the approximation function $\mathbf{w}^h(\mathbf{x})$ can be written as,

$$
\mathbf{w}^h(\mathbf{x}) = \mathbf{\Phi}_{\mathbf{w}}^T(\mathbf{x})\mathbf{w} + \mathbf{\Phi}_{\theta_{\mathbf{x}}}^T\theta_{\mathbf{x}} + \mathbf{\Phi}_{\theta_{\mathbf{y}}}^T\theta_{\mathbf{y}}, \tag{13}
$$

where,

$$
\begin{aligned}
\mathbf{\Phi}_{\mathbf{w}}^T &= \mathbf{p}^T(\mathbf{x})\mathbf{A}^{-1}(\mathbf{x})\mathbf{C}_{\mathbf{w}} \\
\mathbf{\Phi}_{\theta_x}^T &= \mathbf{p}^T(\mathbf{x})\mathbf{A}^{-1}(\mathbf{x})\mathbf{C}_{\theta_{\mathbf{x}}}. \\
\mathbf{\Phi}_{\theta_y}^T &= \mathbf{p}^T(\mathbf{x})\mathbf{A}^{-1}(\mathbf{x})\mathbf{C}_{\theta_{\mathbf{y}}}
\end{aligned} \tag{14}
$$

Thus the equation 13 can be rewritten in matrix form as,

$$
\mathbf{w}^h(\mathbf{x}) = \begin{bmatrix} \mathbf{\Phi}_{\mathbf{w}}^T & \mathbf{\Phi}_{\theta_x}^T & \mathbf{\Phi}_{\theta_y}^T \end{bmatrix} \begin{Bmatrix} \mathbf{w} \\ \theta_x \\ \theta_y \end{Bmatrix} = \mathbf{N}^T\mathbf{d}. \tag{15}
$$

However, due to the lack of Kronecker delta properties in EFGM, imposing essential boundary conditions involves some additional complication. Here scaled transformation method [27] is used, in which the displacement approximations given in equation 13 are scaled using a scaled transformation matrix in such a way that, nodal values and nodal parameters will coincide along the nodes on essential boundary.

In scaled transformation method, an identity matrix say $\mathbf{\Lambda}$ having number of rows and columns equal to the total DOF is constructed. The rows corresponding to the degrees of freedom, in which essential boundary conditions has to be applied, is then populated with shape function associated with it. A representation of $\mathbf{\Lambda}$ can be shown as,

$$
\mathbf{\Lambda} = \begin{Bmatrix}
\phi_{11} & \phi_{12} & \phi_{13} & \phi_{14} & . & . & \phi_{1m} & . & . \\
\phi_{21} & \phi_{22} & \phi_{23} & \phi_{24} & . & . & \phi_{2m} & . & . \\
0 & 0 & 1 & 0 & . & . & 0 & . & . \\
0 & 0 & 0 & 1 & . & . & 0 & . & . \\
. & . & . & . & . & . & . & . & . \\
. & . & . & . & . & . & . & . & . \\
\phi_{n1} & \phi_{n2} & \phi_{n3} & . & . & . & \phi_{nm} & . & . \\
. & . & . & . & . & . & . & . & . \\
. & . & . & . & . & . & . & . & .
\end{Bmatrix}, \tag{16}
$$

where, ϕ_{ij} represents shape function of node i evaluated at node j. Here 1^{st},2^{nd} and n^{th} are rows corresponding to degrees of freedom in which boundary condition has to be applied. Detailed

discussions on this are not included here and reader may advised to go through [27]. Once, $\mathbf{\Lambda}$ is formed, the discretized system of equations can be written from 4 and 15 as,

$$\frac{1}{2}\overline{\mathbf{d}}^T\overline{\mathbf{K_f}\mathbf{d}} + \frac{F_x}{2}\overline{\mathbf{d}}^T\overline{\mathbf{Kg}_x}\overline{\mathbf{d}} + \frac{F_y}{2}\overline{\mathbf{d}}^T\overline{\mathbf{Kg}_y}\overline{\mathbf{d}} + F_{xy}\overline{\mathbf{d}}^T\overline{\mathbf{Kg}_{xy}}\overline{\mathbf{d}} = 0, \tag{17}$$

where, $\overline{\mathbf{K}}$ is the modified stiffness matrix, $\overline{\mathbf{Kg_x}}, \overline{\mathbf{Kg_y}}$ and $\overline{\mathbf{Kg_{xy}}}$ are modified geometric stiffness matrices, given by,

$$\begin{aligned}
\overline{\mathbf{K}} &= \mathbf{\Lambda^{-T} K \Lambda^T} \\
\overline{\mathbf{Kg_x}} &= \mathbf{\Lambda^{-T} Kg_x \Lambda^T} \\
\overline{\mathbf{Kg_y}} &= \mathbf{\Lambda^{-T} Kg_y \Lambda^T} \\
\overline{\mathbf{Kg_{xy}}} &= \mathbf{\Lambda^{-T} Kg_{xy} \Lambda^T},
\end{aligned} \tag{18}$$

where $\mathbf{K_f}$ is stiffness matrix and $\mathbf{Kg}_x, \mathbf{Kg}_y$ and $\mathbf{Kg}_{xy}$ are geometric stiffness matrices. The sign of geometric stiffness terms in the equation depends upon the direction of in-plane loads. The terms will be positive for stretching and negative for compression. Stiffness matrix and geometric stiffness matrices are given by,

$$\begin{aligned}
\mathbf{K_f} &= \iint \mathbf{N}''^T \mathbf{D} \mathbf{N}'' dxdy \\
\mathbf{Kg}_x &= \iint \mathbf{N}_{,x}^T \mathbf{N}_{,x} dxdy \\
\mathbf{Kg}_y &= \iint \mathbf{N}_{,y}^T \mathbf{N}_{,y} dxdy \\
\mathbf{Kg}_{xy} &= \iint \mathbf{N}_{,x}^T \mathbf{N}_{,y} dxdy,
\end{aligned} \tag{19}$$

where $\mathbf{N}''$ represents matrix containing the double derivatives of shape function, $\mathbf{N_{,x}}, \mathbf{N_{,y}}$ represents partial derivative of $\mathbf{N}$ with respect to x, y respectively. Consequently, the essential boundary conditions are imposed simply by following FEM methodology.

MODEL DESCRIPTION

For the present study, four cases are taken in to consideration. Case(a):Wrinkling analysis of homogeneous thin plate subjected to uni-axial compressive loading Case(b): Wrinkling analysis of a pre-stressed, homogeneous membrane, case(c): Wrinkling analysis of non-homogeneous membranes, subjected to linearly varying, uni-axial load. Though inhomogeneity in modulus of elasticity is considered for case(c) and case(d), Poisson's ratio is assumed to be constant. Moreover, for all the cases material is assumed to be isotropic.

Case(a): Wrinkling analysis of a homogeneous thin plate with uni-axial compressive loading

A homogeneous thin plate of dimension $0.3m \times 0.3m$ with thickness $0.2mm$, which is free of any initial pre-stress and loaded with a uni-axial compressive load is considered for the study. The material is assumed to be Kapton which has an Young's modulus of $3500 \times 10^6 N/m^2$ and Poisson's ratio of 0.31. All sides of the membrane are given simply supported (SSSS) boundary condition. The results obtained using EFGM, are compared with analytical solution and the results obtained using different element types in FEM. Analytical solution obtained using Navier's solution method is used here [36]. Five different quadrilateral element types, S4 (four noded element with six DOF per node and with full integration), S4R(four noded element,

with six DOF per node and with reduced integration), S4R5 (four noded element with 5 DOF per node with reduced integration), S8R(8 noded element with six DOF per node and with reduced integration) and S8R5 (8 noded element with 5 DOF per node and with reduced integration) are taken for modeling. For comparison, discretization in EFGM is done with regularly distributed nodes, similar to that of linear element types (S4, S4R and S4R5) in FEM.

Three different modes, first ($m = 1, n = 1$), $20^{th}(m = 5, n = 2)$ and $30^{th}(m = 9, n = 2)$ modes are considered for study, where m, n are number of half sine waves in x, y direction respectively. This is selected with an objective to study the capability of the methods in an initial, an intermediate and a higher mode. Mode shapes of corresponding modes, obtained from EFGM are shown in Fig. 1. A convergence study on eigen values obtained using EFGM and all element types in FEM for the the three different modes under consideration have been carried out.

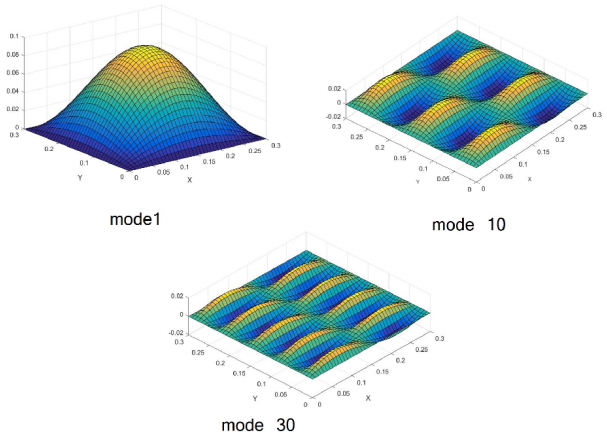

Fig. 1. Mode shapes obtained from EFGM, for wrinkling of membrane without pre-stress and simply supported on all sides

Fig. 2a shows the variation of eigenvalue with number nodes for the the first mode. It can be observed from Fig. 2a that, FEM results obtained from models which uses 4 node quadrilateral elements are showing larger variations from analytical solution when compared to other element types and EFGM, for lower number nodes. However, it is to be noted that the difference from analytical solution for S4 element are is within 2%. Moreover, a convergence is observed while number of nodes are increased. Accurate and consistent results are obtained while 8 node quadrilateral elements and EFGM are used for the analysis for all the set of nodes. Variation of 20^{th} mode eigenvalues with respect to number of nodes is shown in Fig. 2b. From the figure it can be observed that the variation of the results corresponding to element types S8R, S4R, S4R5 and S4 are very large for lesser number of nodes. For higher number of nodes all the element types are providing satisfactory results. However element type S8R5 and EFGM are showing very small error even with the use of lower number of nodes and hence shows a comparatively consistent results. Eigenvalues obtained for higher mode under consideration is given in Fig. 2c.

A large error is observed for all FEM elements at the lesser number of nodes, while EFGM gives fairly accurate and consistent results. Table 1 shows the percentage variation of eigenvalues obtained using EFGM and FEM from analytical solution for the set 121 nodes. It can be observed that S8R is showing a huge variation of 8239.83% and other FEM element types also show unacceptable variation from analytical solution at lesser number of nodes. However EFGM results are within 6%variation from analytical solutions.

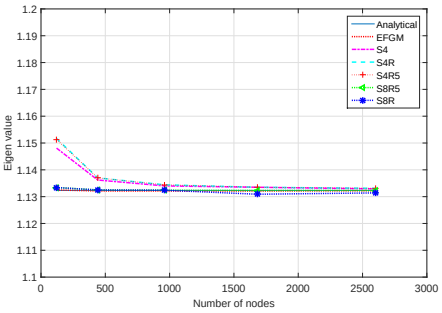

(a) 1^{st} mode($m = 1, n = 1$)

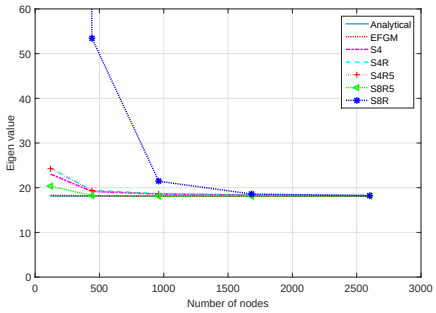

(b) 20^{th} mode($m = 4, n = 4$)

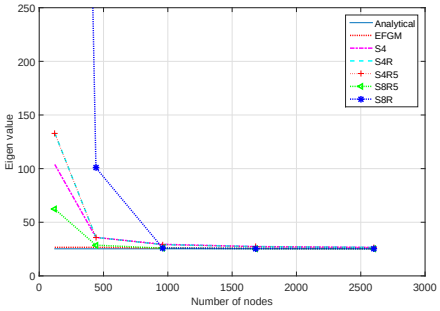

(c) 30^{th} mode($m = 9, n = 2$)

Fig. 2. Variation of 1^{st} mode($m = 1, n = 1$) eigenvalues with number of nodes for the case (a)

Table 1. Percentage variation of eigenvalues from analytical value with the use of 121 nodes for $30th$ mode($m = 9, n = 2$)

Method	Element type	Percentage variation(%)
FEM	S4	311.36
	S4R	427.50
	S4R5	426.36
	S8R	8239.83
	S8R5	146.65
EFGM		5.38

Thus EFGM with only 3 DOF per nodes is observed to provide accurate results with lesser number of nodes compared to FEM with 5 or 6 DOF per node.

Case(b): Wrinkling analysis of a pre-stressed, homogeneous membrane

A pre-stressed homogeneous membrane with same size and material as that of case(a) is considered for analysis. Two different numerical examples are examined in this case. In both the examples, the membrane is being pre-stressed in the y direction and given simply supported boundary condition on all sides. In example(i), Compression induced wrinkling of pre-stressed membrane due to compressive load in x direction Fig. 3a was studied and in example(ii), shear induced wrinkling of pre-stressed membrane as shown in Fig. 3b is studied. Both the problems are analyzed using EFGM and compared with results from FEM analysis using different element types available. Three modes (first mode, and an intermediate mode and a higher mode) are

taken into consideration. A convergence study for eigenvalues corresponds to 1^{st} mode, 20^{th} mode and 30^{th} mode have been carried out for both the examples. Percentage variation of eigenvalues obtained with a reference value is also analyzed for each element type and EFGM for studying the rate of convergence. The reference value is taken as the eigenvalue obtained when maximum number of nodes, that is 3721 nodes, are used. That is, reference value is different for EFGM and every element type.

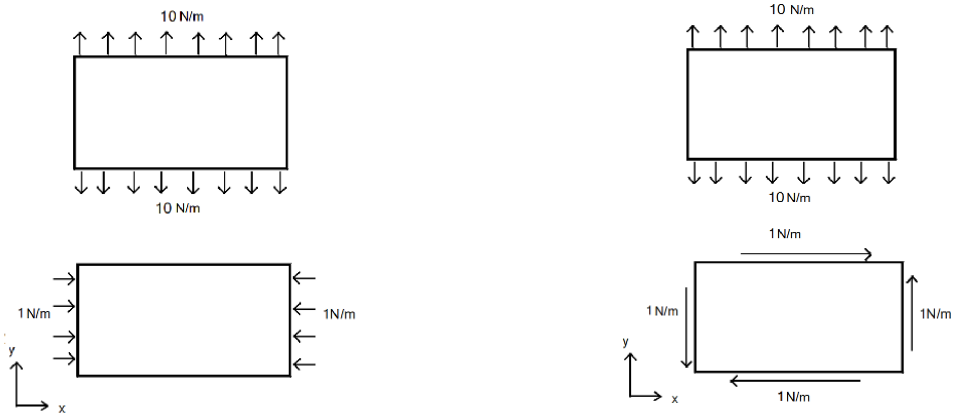

(a) Example 1 **(b)** Example 2

Fig. 3. Problem considered for wrinkling analysis of pre-stressed membrane due to compressive and shear loading

Example 1: Compression induced wrinkling

Wrinkling of a pre-stressed homogeneous membrane due to compressive loading in x axis is analyzed using EFGM and different element types available. A pre stress of $10N/m$ is applied to the membrane initially in y direction. The mode shapes of the modes taken into consideration for study is shown in Fig. 4

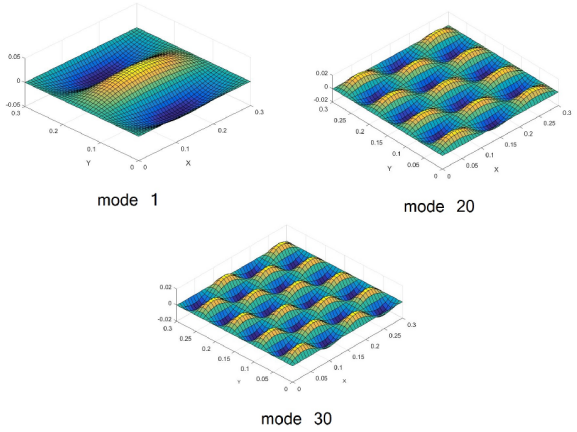

Fig. 4. Mode shapes obtained from EFGM, for wrinkling of pre-stressed membrane due to compressive loading

The results obtained from first mode is shown in Fig. 5a. From Fig. 5a it is clear that for initial mode, all FEM element types and EFGM provides fairly consistent eigenvalues with

respect to number of nodes, except for lowest number of nodes. At lowest number of nodes considered, eigenvalue corresponding to S8R shows high variation. Percentage variation of eigenvalues from reference value for all element types and EFGM are shown in table 2. From Table 2, it can be observed that, except for S8R5 and EFGM all other element types shows error values more than 5% at 121 nodes. S8R is showing very high percentage variation of 71% at 121 number of nodes. But at 441 nodes percentage variation is reduced to 1.54%. For higher number of nodes, all element types and EFGM show consistent result with percentage variation within 0.3%.

For an intermediate mode, as shown in Fig. 5b, element types S8R, S4, S4R and S4R5 of FEM are showing lower convergence rate, while element types S8R5 and EFGM results shows higher convergence rate. The percentage variation of eigenvalues from the reference values are shown in Table 3. From the table it can be observed that element type S8R shows huge variation of 3584.40% with the use of 121 nodes. Element types S4, S4R, S4R5 and S8R5 also shows large variation at lower number of nodes. All element types except S8R shows percentage variation within 5% for number of nodes higher than 961. However, EFGM shows consistent results with percentage variation of 3.76% even at 121 nodes.

For a higher mode, from Fig. 5c, all element types are showing lower rate of convergence compared to EFGM results. EFGM gives consistent results at higher modes. Percentage variation in eigenvalues are shown in Table 4. As element type S8R fails to capture the 30^th mode with the use of 121 nodes, the percentage variation correspond to which is not included in Table 4. From the Table 4, it is clear that element type S8R is showing huge variation at lower number of nodes, element types S4, S4R, S4R5 and S8R5 also show considerable variation with the use of 121 nodes. However EFGM shows more consistent results compared to all element types in FEM.

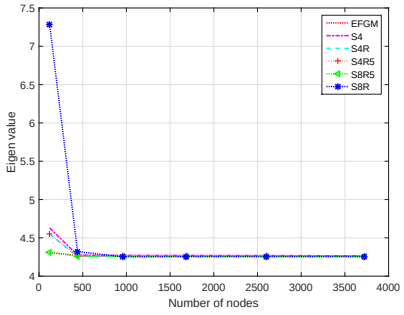

(a) 1^{st} mode

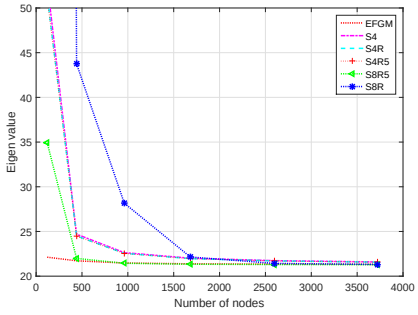

(b) 20^{th} mode

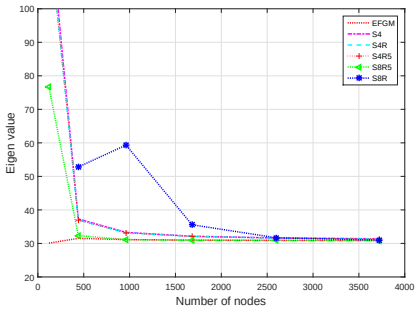

(c) 30^{th}mode

Fig. 5. Variation of eigenvalues with number of nodes for compression induced wrinkling

Table 2. Percentage variation of eigenvalue for 1^{st} mode compressive loading

Method/Element type	Number of nodes					
	121	441	961	1681	2601	3721
S4	8.50	0.22	0.15	0.12	0.10	0
S4R	6.74	0.087	0.04	0.09	0.07	0
S4R5	6.70	0.09	0.04	0.09	0.07	0
S8R5	1.24	0.12	0.04	0.01	0.01	0
S8R	71.2	1.54	0.09	0.02	0.01	0
EFGM	1.26	0.19	0.1	0.04	0.01	0

Table 3. Percentage variation of eigenvalue for 20^{th} mode compressive loading

Method/Element type	Number of nodes					
	121	441	961	1681	2601	3721
S4	144.53	14.38	4.83	1.94	0.67	0
S4R	138.24	13.57	4.55	1.83	0.63	0
S4R5	136.96	13.46	4.51	1.81	0.62	0
S8R5	64.02	3.28	0.72	0.22	0.06	0
S8R	3584.40	105.37	32.20	3.94	0.57	0
EFGM	3.76	1.88	0.72	0.30	0.10	0

Table 4. Percentage variation of eigenvalue for 30^{th} mode compressive loading

Method/Element type	Number of nodes					
	121	441	961	1681	2601	3721
S4	307.72	18.85	6.11	2.43	0.84	0
S4R	293.83	17.93	5.81	2.31	0.79	0
S4R5	289.53	17.73	5.75	2.28	0.79	0
S8R5	148.48	4.85	1.04	0.32	0.09	0
S8R	*	70.27	91.31	14.65	2.16	0
EFGM	2.56	2.04	0.80	0.33	0.16	0

*S8R fails to capture 30^{th} mode at 121 nodes

Example 2: Shear induced wrinkling

Wrinkling of a pre-stressed homogeneous membrane due to shear loading is analyzed using EFGM and FEM. An in-plane pre-tension of $10N/m$ is applied. The mode shapes of the corresponding modes taken into consideration for study is shown in Fig. 6.

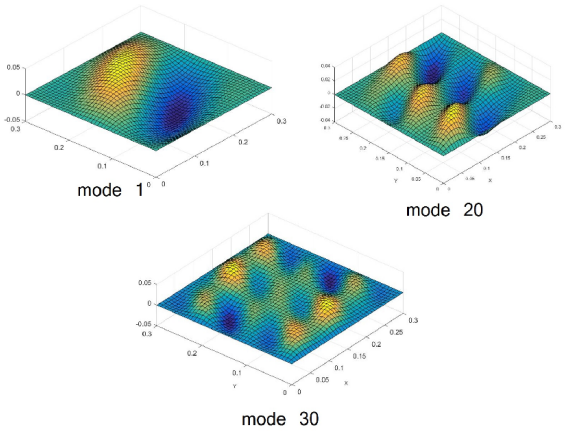

Fig. 6. Mode shapes obtained from EFGM, for wrinkling of pre-stressed membrane due to shear loading

The variation of eigenvalues with the number of nodes for the first mode is shown in Fig. 7a. From Fig. 7a it is observed that, element type S4R and S8R shows less consistency in results at lower number of nodes, while other element types show consistent results. Particularly, element type S8R5 and EFGM shows consistency and high rate of convergence in the results. Table 5 shows percentage variation in eigenvalues of each element types and EFGM at lower number of nodes. It is observed that at 121 nodes all element types except S8R5 and EFGM are show percentage variation higher than 5%. Particularly element type S8R shows a huge variation of 86.13% at 121 nodes. With the use of 441 number of nodes, except for element type S8R, all other element types and EFGM has percentage variation value within 3%. Particularly, element type S8R5 and EFGM shows very low percentage variation of 0.12% and 0.21 % respectively.

Fig. 7b shows the variation in 20^{th} mode eigenvalues for shear induced wrinkling. From Fig. 7b it is observed that, all element types except S8R5 shows inconsistent results. Also EFGM provides faster rate of convergence compared to all element types. Table 6 shows the percentage variation of 20^{th} mode eigenvalues with number of nodes. As element type S8R fails to capture 20^{th} mode, the results corresponding to which is not included in Table 6 and Fig. 7b. From the Table 6, it is clear that EFGM shows very low percentage variation and higher rate of convergence compared to all element types in FEM.

Fig. 7c shows the variation of eigenvalues corresponding to the higher mode under consideration with respect to total number of nodes used for discretization. It can be clearly observed that only EFGM is able to produce consistent results irrespective of the number of nodes, in comparison with FEM. Table 7 shows the percentage variation of eigenvalues for all the elements types in FEM and EFGM for different set of nodes with respect to its own reference value. It is very much clear from the table that EFGM shows faster rate of convergence with consistent result at higher modes too. FEM results are highly dependent on the number of nodes and element types used. Similar to 20^{th} mode results, element type S8R fails to capture 30^{th} mode also at 121 number of nodes

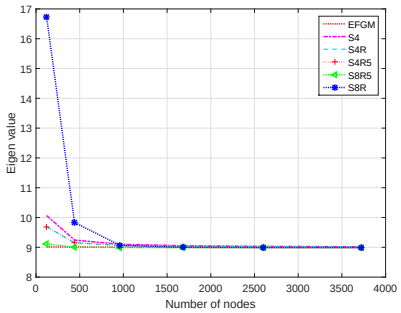

(a) 1^{st} mode

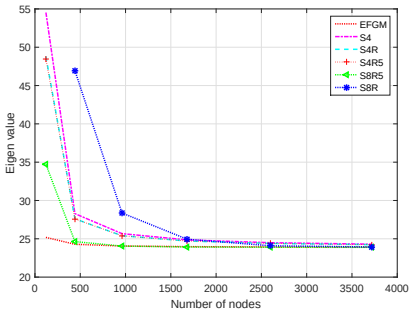

(b) 20^{th} mode

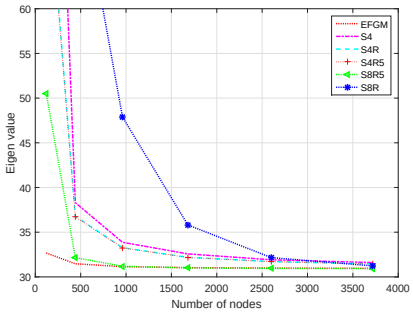

(c) 30^{th}mode

Fig. 7. Variation of eigenvalues with number of nodes for for shear induced wrinkling

Table 5. Percentage variation of eigenvalue for 1^{st} mode shear loading

Method/Element type	Number of nodes					
	121	441	961	1681	2601	3721
S4	11.63	2.49	0.92	0.38	0.13	0
S4R	7.61	1.62	0.60	0.25	0.09	0
S4R5	7.52	1.60	0.59	0.24	0.08	0
S8R5	1.42	0.12	0.03	0.01	0.01	0
S8R	86.13	9.39	0.85	0.10	0.01	0
EFGM	0.22	0.21	0.08	0.03	0.01	0

Table 6. Percentage variation of eigenvalue for 20^{th} mode shear loading

Method/Element type	Number of nodes					
	121	441	961	1681	2601	3721
S4	124.43	13.92	5.66	2.30	0.80	0
S4R	101.34	13.92	4.83	1.96	0.68	0
S4R5	100.02	13.82	4.80	1.94	068	0
S8R5	45.40	3.13	0.68	0.2	0.06	0
S8R	*	96.23	18.56	4.24	0.69	0
EFGM	5.31	1.54	0.60	0.25	0.09	0

*S8R fails to capture 20^{th} mode at 121 nodes

Table 7. Percentage variation of eigenvalue for 30^{th} mode shear loading

Method/Element type	Number of nodes					
	121	441	961	1681	2601	3721
S4	283.14	21.22	7.20	3.09	1.01	0
S4R	146.12	16.91	5.76	2.32	0.81	0
S4R5	143.88	16.72	5.67	2.32	0.81	0
S8R5	63.36	3.98	0.86	0.26	0.01	0
S8R	*	146.58	53.33	14.67	2.96	0
EFGM	5.55	1.64	0.61	0.25	0.09	0

*S8R fails to capture 30^{th} mode at 121 nodes

Thus it can be concluded that in wrinkling analysis of pre-stressed membrane, EFGM shows rate of convergence and consistent results, while the values obtained using FEM are highly dependent on the element type and size used.

Case(c):Wrinkling analysis of non-homogeneous membrane, subjected to linearly varying, uni-axial load

Wrinkling analysis of non-homogeneous membrane, subjected to linearly varying, uni-axial compressive load as shown in Fig. 8 is carried out using EFGM. The load F_x is taken as zero and F_y is taken as compressive and linearly varying along edges $y = 0, y = b$.

The variation of F_y is given by [20],

$$F_y = -F_0(1 - \gamma\overline{x}), \tag{20}$$

where γ is the loading parameter. F_0 is the load at $\overline{x} = 0$, where $\overline{x}$ is given by,

$$\overline{x} = \frac{x}{a} \tag{21}$$

similarly for consistency other non-dimensional parameters are defined as,

$$\begin{aligned} \overline{h} &= \frac{h}{a} \\ F_0^* &= \frac{12F_0(1-\nu^2)}{aE_0\overline{h}^3}, \end{aligned} \tag{22}$$

where, a, b and h are length, width and thickness of the membrane respectively. F_0^* is the non-dimensional force parameter. The modulus of elasticity E_0, is assumed to be exponentially varying, which is given by,

$$E = E_0 e^{\mu\overline{x}} \tag{23}$$

where μ is the non-homogeneity parameter.

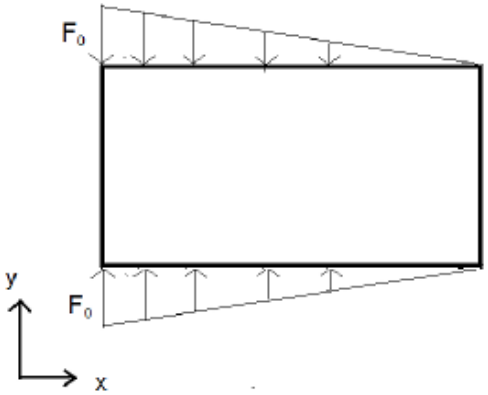

Fig. 8. Problem taken for non-homogeneous membrane wrinkling analysis

A non-dimensional critical force parameter is defined as [20],

$$F^*_{0cr} = \frac{12F_{0cr}(1-\nu^2)}{aE_0\overline{h}^3}, \tag{24}$$

where F_{0cr} is the critical load obtained from wrinkling analysis.

Two type of boundary conditions are taken for analysis. In both of the cases, loading side is given simply supported boundary condition ($y = 0$ and $y = b$). In the first case, the other two supports are considered clamped (C-C). In the second problem, one of the non-loading edge is given clamped support and the other edge is given simply supported (C-SS) boundary condition. Analysis are done for two different loading parameters, $\gamma = 0$ ie uniform loading and $\gamma = 1$ ie, linearly varying loading from maximum value F_0 at $\overline{x} = 0$ to zero at $\overline{x} = 1$. Table 8 and Table 9 shows a comparison of critical force parameter obtained using EFGM for different values of non-homogeneous parameter, μ. The same problem has been solved by [20] by DQ method. Here results available in [20] is taken for comparison. Table 8 shows the results for $b/a = 1$ and $\gamma = 0$ and Table 9 shows the results of $b/a = 1$ and $\gamma = 1$

Table 8. A comparison of critical force parameter for $b/a = 1$ and $\gamma = 0$, obtained using EFGM and using DQ given in[20] for different values of non-homogenity parameter, μ

μ	C-SS		C-C	
	EFGM	[20]	EFGM	[20]
-0.5	43.9491	43.9425	58.8788	66.0304
-0.3	48.6693	48.6598	65.2750	73.0507
0	56.6673	56.6536	75.9725	84.9225
0.3	65.9110	65.8938	88.1120	98.6082
0.5	72.8551	72.8365	97.0748	108.8660

Table 9. A comparison of critical force parameter for $b/a = 1$ and $\gamma = 1$, obtained using EFGM and using DQ given in [20] for different values of non-homogenity parameter, μ

μ	C-SS		C-C	
	EFGM	[20]	EFGM	[20]
-0.5	61.5015	61.4897	117.7998	133.780
-0.3	67.8166	67.8000	128.2408	146.139
0	78.4570	78.4334	145.34	166.7380
0.3	90.6731	90.6433	164.2914	190.086
0.5	99.8002	99.7673	178.0288	207.3480

From the Table 8 and 9 it can be observed that for membrane with C-SS boundary conditions, EFGM provides matching F^*_{0cr} values with the reference value. However, for membrane with C-C boundary conditions EFGM results do not match with the reference values available in literature. Hence for comparison, a homogeneous membrane whose results are available in literature [17, 19] is taken into consideration. F^*_{0cr} values obtained for homogeneous membrane ($\mu = 0$) of b/a ratio 1 and $\gamma = 0$, with C-C boundary conditions using different methods are shown in table 10. It can be observed that, EFGM results match well with that obtained using all methods except that available in *et al*[20]. Hence, it is evident from table 10 that results of C-C boundary condition shown in [20] is erroneous and that is the reason for mismatch of results in table 8 and table 9 for C-C boundary condition.

Table 10. A comparison of critical force parameter for $b/a = 1$ and $\gamma = 0$ for a homogeneous($\mu = 0$) membrane

Method	F^*_{0cr}
EFGM (1296 nodes)	75.9725
Power series ([17])	75.9100
DQM ([19])	75.9100
DQM([20])	84.9225

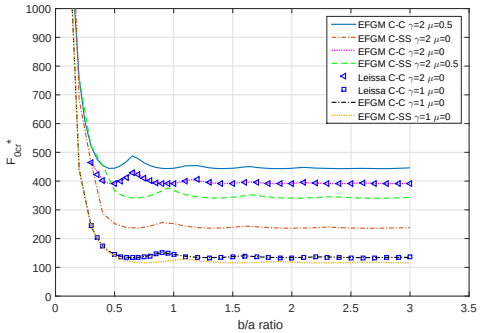

Fig. 9. Wrinkling curves for different cases of study using EFGM.

Wrinkling curves for non-homogeneous membrane corresponds to four combinations of μ and boundary conditions (C-C membrane with $\mu = 0$, C-SS membrane with $\mu = 0$, C-C membrane with $\mu = 0.5$ and C-SS membrane with $\mu = 0.5$) are shown in Fig. 9. Wrinkling

curve for a homogeneous membrane with $\mu = 0$ and loading parameter $\gamma = 2$ and $\gamma = 1$, are available in [17]. From the Fig. 9, it can be observed that, the curves plotted using EFGM are found to match with that available in [17].

Case(d): Wrinkling analysis of pre-stressed non-homogeneous membrane due to compressive load

Compression induced wrinkling of non-homogeneous membrane pre-stressed by $10N/m$ in y direction is considered for study. Membranes with non-homogeneity parameter μ equal to 0.3 and 0.5 and boundary conditions C-C and C-SS are considered. Initial, intermediate and higher modes of wrinkling is examined for all these four cases and the resulting plots showing the variation of eigenvalues with respect to number of nodes are shown in Fig. 10. From the figure it is clear that EFGM shows a faster rate of convergence in results for all the three modes taken into consideration. It is observed that, though at 121 nodes eigenvalues corresponds to 1^{st} and 20^{th} modes shows variation within 5%, eigenvalue corresponds to 30^{th} mode shows a variation of 30% with respect to converged value. However, as number of nodes are increased to 441, variation in all the modes are reduced to 3% or less. It is also found that, in pre-stressed case, the eigenvalues obtained for C-C boundary condition and C-SS boundary condition do not show much difference at higher modes. Also as expected, it is observed that, with the increase in μ value, the eigenvalue also increases.

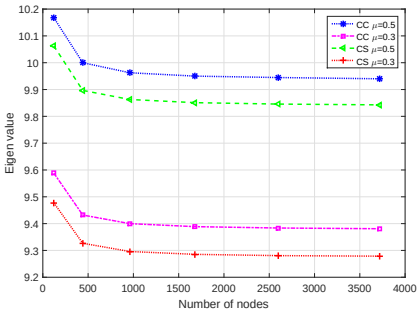

(a) 1^{st} mode

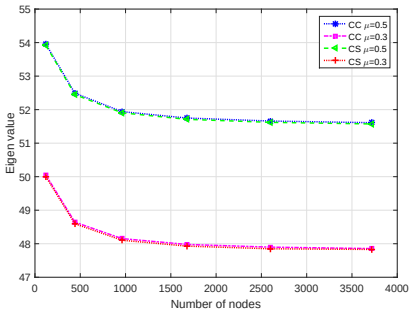

(b) 20^{th} mode

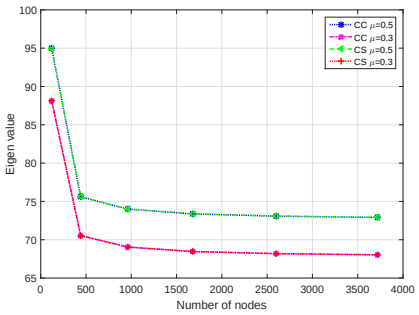

(c) 30^{th} mode

Fig. 10. Variation of eigenvalue with number of nodes for pre-stressed non-homogeneous membrane

CONCLUSION

The current work discusses the use of EFGM, a meshless method, for wrinkling analysis of pre-stressed membranes and proves its capabilities in capturing the eigenvalues even at higher modes. Classical plate formulation with three DOF per node is considered for study.

A general EFGM formulation for non-homogeneous membrane with in-plane loads derived by considering the bending stiffness, though it is negligible. Initially, a simple wrinkling analysis of homogeneous thin plate due to uni-axial compressive load is carried out and compared with analytical and FEM solutions to validate the proposed method. The results shows that, EFGM provides accurate results for all the modes under consideration, even with the use of less number of nodes. Further, wrinkling analysis of pre-stressed membrane due to shear and compressive loading is studied. The results obtained from both these problems are compared with result obtained from that of FEM using different element types. A study on consistency of the numerical tools are also conducted by taking respective converged eigenvalues as reference for every element types and EFGM. It is found that, consistent results adn faster rate of convergence are obtained when EFGM is employed regardless of modes under consideration. However many FEM element types shows larger variation at lower number of nodes at higher modes. The study is further extended to wrinkling analysis of non-homogeneous membrane subjected to linearly varying in-plane load, to demonstrate the capability of the proposed method. The results obtained matches well with the results available in the literature. Moreover wrinkling curves for non-homogeneous membranes are proposed. Finally, EFGM is used for wrinkling analysis of pre-stressed non-homogeneous membrane for two different non-homogeneity parameter and boundary conditions.It is observed that, EFGM produces consistent results and shows a faster rate of convergence. Thus, EFGM is proved to be an efficient and accurate numerical tool which can be used for wrinkling analysis of membranes.

REFERENCES

[1] David Sleight, Yuki Michii, David Lichodziejewski, Billy Derbes, Troy Mann, Kara Slade, and John Wang. Finite element analysis and test correlation of a 10-meter inflation-deployed solar sail. In *46th AIAA/ASME/ASCE/AHS/ASC Structures, Structural Dynamics and Materials Conference*, page 2121, 2005.

[2] Christopher Talley, William Clayton, Paul Gierow, Greg Laue, Jennie McGee, and James Moore. Advanced membrane materials for improved solar sail capabilities. In *43rd AIAA/ASME/ASCE/AHS/ASC Structures, Structural Dynamics, and Materials Conference*, page 1561, 2002.

[3] Herbert Wagner. Flat sheet metal girders with very thin metal web. *Z. Flugtechn. Motorluftschiffahrt*, 20:200–314, 1929.

[4] Eric Reissner. On tension field theory. *Proc. of the 5th Int. Congr. for Applied Mechanics Harvard Univ. & MIT*, pages 88–92, 1938.

[5] Manuel Stein and John M Hedgepeth. *Analysis of partly wrinkled membranes*. National Aeronautics and Space Administration Washington, 1961.

[6] E H Mansfield. Tension field theory, a new approach which shows its duality with inextensional theory [c]. In *Proceeding XII International Congress of Applied Mechanics*, pages 305–320, 1968.

[7] Chien H Wu and Thomas R Canfield. Wrinkling in finite plane-stress theory. *Quarterly of Applied Mathematics*, 39(2):179–199, 1981.

[8] Allen C Pipkin. The relaxed energy density for isotropic elastic membranes. *IMA journal of applied mathematics*, 36(1):85–99, 1986.

[9] D J Steigmann. Tension-field theory. In *Proceedings of the Royal Society of London A: Mathematical, Physical and Engineering Sciences*, volume 429, pages 141–173. The Royal Society, 1990.

[10] Wesley Wong and Sergio Pellegrino. Wrinkled membranes i: experiments. *Journal of Mechanics of Materials and Structures*, 1(1):3–25, 2006.

[11] Wesley Wong and Sergio Pellegrino. Wrinkled membranes ii: analytical models. *Journal of Mechanics of Materials and Structures*, 1(1):27–61, 2006.

[12] Wesley Wong and Sergio Pellegrino. Wrinkled membranes iii: numerical simulations. *Journal of Mechanics of Materials and Structures*, 1(1):63–95, 2006.

[13] Wei-wei Xiao, Wu-jun Chen, and Gong-yi Fu. Wrinkle analysis of a space planar film reflect-array. *Journal of Zhejiang University-SCIENCE A*, 12(1):24–32, 2011.

[14] Satish Kumar, S H Upadhyay, and Anil C Mathur. Wrinkling simulation of membrane structures under tensile and shear loading. *Journal of Vibration Analysis*, 3(1):17–33, 2015.

[15] Y Tomita and A Shindo. Onset and growth of wrinkles in thin square plates subjected to diagonal tension. *International Journal of Mechanical Sciences*, 30(12):921–931, 1988.

[16] Tomoshi Miyamura. Wrinkling on stretched circular membrane under in-plane torsion:: bifurcation analyses and experiments. *Engineering Structures*, 22(11):1407–1425, 2000.

[17] Arthur W Leissa and Jae-Hoon Kang. Exact solutions for vibration and buckling of an ss-c-ss-c rectangular plate loaded by linearly varying in-plane stresses. *International Journal of mechanical sciences*, 44(9):1925–1945, 2002.

[18] Jae-Hoon Kang and Arthur W Leissa. Exact solutions for the buckling of rectangular plates having linearly varying in-plane loading on two opposite simply supported edges. *International Journal of Solids and Structures*, 42(14):4220–4238, 2005.

[19] Xinwei Wang, Lifei Gan, and Yongliang Wang. A differential quadrature analysis of vibration and buckling of an ss-c-ss-c rectangular plate loaded by linearly varying in-plane stresses. *Journal of Sound and Vibration*, 298(1):420–431, 2006.

[20] Roshan Lal and Renu Saini. Buckling and vibration of non-homogeneous rectangular plates subjected to linearly varying in-plane force. *Shock and Vibration*, 20(5):879–894, 2013.

[21] Vishal Nayyar, K Ravi-Chandar, and Rui Huang. Stretch-induced stress patterns and wrinkles in hyperelastic thin sheets. *International Journal of Solids and Structures*, 48(25):3471–3483, 2011.

[22] P Frank Pai. *Highly flexible structures: modeling, computation, and experimentation*. AIAA (American Institute of Aeronautics & Ast, 2007.

[23] OC Zienkiewicz and RL Taylor. *The Finite Element Method. Solid and Fluid Mechanics. Dynamics and Non-Linearity, Vol. II*. McGraw-Hill, New York, 1991.

[24] Gui Rong Liu and Yuan Tong Gu. *An introduction to meshfree methods and their programming*. Springer Science & Business Media, 2005.

[25] Ted Belytschko, Yun Yun Lu, and Lei Gu. Element-free galerkin methods. *International journal for numerical methods in engineering*, 37(2):229–256, 1994.

[26] John Dolbow and Ted Belytschko. An introduction to programming the meshless element free galerkin method. *Archives of computational methods in engineering*, 5(3):207–241, 1998.

[27] C O Arun, B N Rao, and S M Srinivasan. Continuum damage growth analysis using element free galerkin method. *Sadhana*, 35(3):279–301, 2010.

[28] Peter Lancaster and Kes Salkauskas. Surfaces generated by moving least squares methods. *Mathematics of computation*, 37(155):141–158, 1981.

[29] Petr Krysl and Ted Belytschko. Analysis of thin plates by the element-free galerkin method. *Computational Mechanics*, 17(1):26–35, 1995.

[30] Petr Krysl and Ted Belytschko. Analysis of thin shells by the element-free galerkin method. *International Journal of Solids and Structures*, 33(20-22):3057–3080, 1996.

[31] C M Tiago and Vitor M A Leitao. Analysis of free vibration problems with the element-free galerkin method. In *Proceedings of the 9th International Conference on Numerical Methods in Continuum Mechanics*, 2003.

[32] L Liu, L P Chua, and D N Ghista. Element-free galerkin method for static and dynamic analysis of spatial shell structures. *Journal of sound and vibration*, 295(1):388–406, 2006.

[33] Ehsan Bahmyari, Mohammad Mahdi Banatehrani, Mohammad Ahmadi, and Marzieh Bahmyari. Vibration analysis of thin plates resting on pasternak foundations by element free galerkin method. *Shock and Vibration*, 20(2):309–326, 2013.

[34] G R Liu and K Y Yang. A penalty method for enforce essential boundary conditions in element free galerkin method. In *Proc. 3rd HPC Asia*, volume 98, pages 715–721, 1998.

[35] Eduard Ventsel and Theodor Krauthammer. *Thin plates and shells: theory: analysis, and applications*. CRC press new york, 2001.

[36] Stephen P Timoshenko and Sergius Woinowsky-Krieger. *Theory of plates and shells*. McGraw-hill, 1959.